

# MOLECULAR DYNAMICS INVESTIGATION INTO THE EFFECT OF PHOSPHORUS NUCLEAR SPIN STATE ON THE PYROPHOSPHATASE-CATALYZED HYDROLYSIS OF PYROPHOSPHATE

ANDY STOKELY AND LANE VOTAPKA

ABSTRACT. A recently developed quantum mechanical model of cognition theorizes that neuronal signaling is significantly influenced by entangled Posner molecules ( $\text{Ca}_9(\text{PO}_4)_6$ ) in the brain. According to this model, entangled Posner molecules form upon the inorganic pyrophosphatase-mediated hydrolysis of singlet pyrophosphate, which produces two entangled phosphates. These entangled phosphates then coordinate with surrounding  $\text{Ca}^{2+}$  and other entangled phosphate molecules to form the S6 symmetric Posner molecule, which is presumed to serve as a qubit for neuronal signaling. This theory assumes that the hydrolysis of pyrophosphate significantly favors singlet pyrophosphate due to its ability to freely rotate while in the binding pocket of pyrophosphatase. However, to our knowledge, this assumption has never been tested. Using molecular dynamics, we were able to conclude that singlet pyrophosphate does not rotate within a timescale of  $1 \mu\text{s}$  while present in the pocket of pyrophosphatase. These results call into question the role of nuclear spin in the specificity of the pyrophosphatase-mediated hydrolysis of pyrophosphate.

## 1. INTRODUCTION

While seldom taken into consideration, ligand nuclear spin can significantly affect both the selectivity and rate of enzymatic reactions [1] [2] [3]. One way that ligand nuclear spin may affect reaction specificity is through the effect that the nuclear spin state of a molecule has on its rotational freedom. This nuclear-dependent rotational parameterization is especially relevant for symmetric molecules that have two spin  $\frac{1}{2}$  nuclei about the axis of symmetry, such as pyrophosphate ( $\text{PP}_i$ ) [4]. A symmetric quantum system with 2 spin  $\frac{1}{2}$  nuclei has three unique triplet nuclear spin states

$$(1) \quad \mathcal{X}_t(\alpha, \beta) = \begin{cases} |t_+\rangle = |\uparrow\uparrow\rangle \\ |t_-\rangle = |\downarrow\downarrow\rangle \\ |t_0\rangle = \frac{|\uparrow\downarrow\rangle + |\downarrow\uparrow\rangle}{\sqrt{2}}, \end{cases}$$

and one singlet spin state

$$(2) \quad \mathcal{X}_s(\alpha, \beta) = |s\rangle = \frac{|\uparrow\downarrow\rangle - |\downarrow\uparrow\rangle}{\sqrt{2}},$$

where  $\alpha$  is the spin variable for the first phosphorus nucleus and  $\beta$  is the spin variable for the second phosphorus nucleus. Symmetry-wise, the three triplet states are all symmetric, while the singlet

---

*Date:* Spring 2019.

state is antisymmetric. Since phosphorus nuclei are fermions, they are subjected to the antisymmetry principle

$$(3) \quad \Psi(q_1, q_2) = -\Psi(q_2, q_1),$$

where  $q_1$  and  $q_2$  are vectors of position and spin variables, which requires the sign of the total wave eigenfunction to change following an exchange of the phosphorus nuclei [5]. In the specific case of  $\text{PP}_i$ , the total angular momentum is a normalized superposition of the singlet and triplet states

$$(4) \quad \Psi_{\text{PP}_i} = \psi_s(\mathbf{r}) \mathcal{X}(\alpha, \beta)_s + \psi_t(\mathbf{r}) \mathcal{X}(\alpha, \beta),$$

where the singlet and triplet spatial eigenfunctions  $\psi_{s,t}(\mathbf{r})$  are approximated by the spherical harmonics  $Y_m^l(\theta, \phi)$ , as depicted in Figures 1 and 2 [6] [7].

Since the singlet spin state is antisymmetric, its spatial component of the wave function is required to be even, and for the triplet spin state, which is symmetric, the spatial component of the wave function must be antisymmetric. This symmetry stipulation leads to singlet rotational states limited to spherical harmonics with even  $\ell$  values, and the triplet spherical harmonics having odd  $\ell$  values. Under normal conditions where  $\text{PP}_i$  is freely tumbling in the extracellular matrix,  $\Psi_{\text{PP}_i}$  is the superposition of the singlet and triplet states. However, when  $\text{PP}_i$  binds in the pocket of pyrophosphatase, its angular momentum  $L \sim 0$  and the spin eigenfunction for  $\text{PP}_i$  reduces either to the pure singlet or pure triplet state. The minimum triplet spherical harmonic results in triplet  $\text{PP}_i$  having extremely constrained rotational freedom. The opposite is true for the singlet state [6] [1] [7].

In certain circumstances, these differences in rotational freedom would be expected to affect the specificity of enzymatic catalysis. One of these situations would be if the enzymatic reaction is dependent on  $\text{H}_2\text{O}$  being able to access the binding pocket, which is often the case for bio-organic hydrolysis reactions [8]. However, recent *ab initio* studies examining the mechanism of the pyrophosphatase-catalyzed hydrolysis of  $\text{PP}_i$  strongly suggest that this enzymatic catalysis does not follow this common trend [9]. Though the hydrolysis of  $\text{PP}_i$  is dependent on the presence of 9  $\text{H}_2\text{O}$ , 8 of the  $\text{H}_2\text{O}$  are believed to coordinate with 4 magnesiums that surround the binding pocket and only one  $\text{H}_2\text{O}$  is actually required to be present in the pocket for hydrolysis to take place, (see Figure 3) [9].

A recently proposed quantum mechanical cognition model by Fisher et. al. [10] assumes that the hydrolysis of pyrophosphate significantly favors singlet  $\text{PP}_i$ . However, the hydrolysis of  $\text{PP}_i$  is dependent on only one hydroxide  $\text{OH}^-$  being present just outside the binding pocket of pyrophosphatase [9]. This eliminates the requirement that the rotational freedom of the  $\text{PP}_i$  expands the space within the binding site to accommodate the  $\text{H}_2\text{O}$  molecules required in Fisher's original model, which suggests that the freedom of rotation, and by extension the nuclear spin state, may not affect the rate of hydrolysis as Fisher originally proposed.

In order to test the rotational freedom of the singlet and triplet nuclear spin states, we used molecular dynamics (MD) to classically simulate the rotation of both constrained  $\text{PP}_i$  and unconstrained  $\text{PP}_i$  in the binding pocket of pyrophosphate. The constrained  $\text{PP}_i$  represented the triplet state, and the unconstrained  $\text{PP}_i$  represented the singlet state. The time scale of rotation of  $\text{PP}_i$  was then measured following the completion of both of the singlet and triplet simulations, and these results were used to determine if  $\text{PP}_i$  rotates in the pocket.

## 2. MATERIALS AND METHODS

In order to determine the hydrolysis of  $PP_i$ 's dependence on the rotational freedom of  $PP_i$ , two MD simulations, one with singlet  $PP_i$  in the binding pocket of pyrophosphatase and one with triplet  $PP_i$  in the binding pocket, were run and the rotation of singlet  $PP_i$  throughout the simulation was measured. A pyrophosphatase homology model constructed from an inorganic pyrophosphatase human sequence [11] and Escherichia coli (E. coli) pyrophosphatase structure (2AUU) [12] was used as the enzyme in all of the MD simulations [13] [14] [15]. Topology files for  $PP_i$  and pyrophosphatase were generated using the force field parameterization programs Antechamber and LEaP, which are part of the AmberTools18 MD suite [16] [17] [18].

After generating the simulation's topology files, the system was simulated using constant pressure MD (NPT) with the MD suite OpenMM [19]. The NPT simulation was run to relax the system's density and to generate box vectors for the following constant volume MD simulation (NVT) [20]. Following the completion of the NPT simulation, two 1  $\mu$ s NVT simulations, one with singlet  $PP_i$  and one with triplet  $PP_i$ , were run using OpenMM [19] in order to determine if singlet  $PP_i$  rotates while it is present in the pocket of pyrophosphatase. In the singlet NVT simulation,  $PP_i$  was unconstrained, which represented the freedom of rotation that singlet  $PP_i$  possesses, while the lack of rotational freedom of the triplet  $PP_i$  was simulated by adding a CustomBondForce. The restraints were added between the first  $PP_i$  phosphorus in the topology file (P1) and the magnesium whose resid is 293 (MG293), and also the second phosphorus (P2) and the magnesium whose resid is 294 (MG294) [19] [21]. All of the parameters that were used in the NPT and NVT simulations are listed in Table 1. Upon completion of the singlet NVT simulation, the distances between P1-MG293 and P2-MG294 were measured at each of the simulation's frames using the MD simulation analysis package CPPTraj [22], and these results were used to determine if singlet  $PP_i$  rotates while it is present in the pocket of pyrophosphatase.

	<b>Singlet</b>	<b>Triplet</b>
<b>Water box (truncated octahedron)</b>	TIP4PEW	TIP4PEW
<b>Force field</b>	AMBER ff14SB	AMBER ff14SB
<b>Temperature</b>	310 K	310 K
<b>Pressure (NPT)</b>	1 bar	1 bar
<b>Barostat (NPT)</b>	MonteCarloBarostat	MonteCarloBarostat
<b>Simulation Length (NPT)</b>	$0.2 * 10^{-9}$ s	$0.2 * 10^{-9}$ s
<b>Simulation Length (NVT)</b>	$1.0 * 10^{-6}$ s	$1.0 * 10^{-6}$ s
<b>Integrator</b>	Langevin	Langevin
<b>Platform</b>	CUDA	CUDA
<b>NonBondedMethod</b>	PME	PME
<b>Constraints</b>	HBonds	HBonds
<b>P-Mg Rotational Constraints (NVT)</b>	none	P1-MG293
<b>P-Mg Constraint Friction Coefficient (NVT)</b>	none	$25.0 \frac{\text{kcal}}{\text{mol} \cdot \text{\AA}}$
<b>P-Mg Constraint Radius (NVT)</b>	none	3.0 $\text{\AA}$

TABLE 1. The conditions, constraints, and parameters that were used for running the singlet and triplet simulations.

### 3. RESULTS

The time scale of  $PP_i$  rotation is depicted in Figure 4. No rotation of  $PP_i$  was observed over the course of the entire 1  $\mu s$  simulation. The spikes in Figure 4 represent the movement of the magnesiums, not the rotation of  $PP_i$ . Figures 5 and 6, show the distance between MG293 and P1 in two consecutive frames in the NVT singlet simulation. The average distance between P1 and MG293 during the singlet simulation was  $3.46 \pm 0.07 \text{ \AA}$ , while the average distance between P1 and MG293 during the triplet simulation was  $3.26 \pm 0.01 \text{ \AA}$  [23] [24].

### 4. DISCUSSION

The results from the singlet simulation show that the average distance between MG293 and P1 is  $3.46 \pm 0.07 \text{ \AA}$ , while the average distance between the same atoms in the triplet simulation is  $3.26 \pm 0.07 \text{ \AA}$  (difference of 5.78%). Furthermore, the singlet distance results had a standard deviation of a 0.07, which shows that distance between MG293 and P1 remained extremely close to the mean distance of  $3.46 \text{ \AA}$  throughout the entire simulation, it was visually confirmed that no  $PP_i$  rotations occurred. Figure 4 does show that there were multiple spikes in distance between P1 and MG293 during the singlet simulation, but these sudden changes in distance were not sustained and were later found to be due to the movement of MG293 during the simulation. The relevance of these results to the proposed mechanism in the referenced quantum cognition model [10] is that they strongly suggest that the hydrolysis of  $PP_i$  does not depend on the rotational freedom of  $PP_i$ , and thus does not likely selectively favor singlet  $PP_i$ .

The quantum mechanical phenomenon of entanglement can only take place, to any appreciable extent, in a biological setting [7], between two identical spin  $\frac{1}{2}$  nuclei, while they are in their singlet state. Since this hydrolytic mechanism does not selectively favor singlet  $PP_i$ , the originally expected yield of approximately 100% entangled  $P_i$  is likely to be hydrolyzed indiscriminately. If singlet  $PP_i$  is selectively hydrolyzed, then it would be due to a mechanism other than rotation affecting pocket shape and water accessibility.

MD is classical approximation of a quantum mechanical system, and aside from the conventional forcefield, we approximated the affect of nuclear spin on available rotational states by using classical restraints. Since the method we used is a classical approximation, some quantum effects have been neglected. It is possible that these quantum effects would have a significant effect on our conclusions [5] [1], but it is reasonable to assume that the timescale of rotation of  $PP_i$  in this classical system would not be significantly different from that of the quantum system. Additionally, MD is the only existing viable method to address  $PP_i$  rotation in a system of this size over a  $\mu s$  timescale.

Since an X-ray crystal structure of inorganic human pyrophosphatase was not available, we used its sequence in combination with a reference crystal structure of *E. coli* inorganic pyrophosphatase (PDBID: 2AUU) to construct a homology model [13]. Due to the high sequence similarity (84% in the binding site of the two sequences), we may assume that the generated homology model is likely to be very close to the actual human inorganic pyrophosphatase structure.

### 5. ACKNOWLEDGEMENTS

The authors would like to thank Heidi Doss, Ariane Jansma, Breeann Kirby along with the rest of the Point Loma Nazarene University STEM Departments for the continuous support they offered throughout this entire research project. Andy Stokely would also like to thank his parents. This research was funded by the Point Loma Nazarene Department of Chemistry and Research Associates.

## REFERENCES

- [1] A. Gutteridge, "Understanding the relationship between enzyme structure and catalysis (unpublished doctoral dissertation)," *Darwin College, Cambridge, United Kingdom.*, 2015.
- [2] J. K. Hwang and A. Warshel, "How important are quantum mechanical nuclear motions in enzyme catalysis?," *J. Am. Chem. Soc.*, vol. 118, pp. 11745–11751, 1996.
- [3] M. Molina-Espiritu, R. Esquivel, S. López-Rosa, and J. S. Dehesa, "Quantum entanglement and chemical reactivity," *Journal of Chemical Theory and Computation*, vol. 11, pp. 5144–5151, 2015.
- [4] A. Cotton, "Chemical applications of group theory," *New York, NY: Wiley-Interscience*, 1990.
- [5] A. Carrington and A. D. McLachlan, "Introduction to magnetic resonance with applications to chemistry and chemical physics," *New York, NY: Harper & Row*, 1967.
- [6] W. R. Johnson, "Lectures on atomic physics," *Notre Dame, Indiana: Notre Dame University Department of Physics.*, 2006.
- [7] R. R. Puri, "Non-relativistic quantum mechanics," *Cambridge, United Kingdom: Cambridge University Press*, 2017.
- [8] A. Williams, "Concerted organic and bio-organic mechanisms," *Boca Raton, FL: CRC Press*, 2000.
- [9] L. Yang, R.-Z. Liao, G.-G. Yu, and R.-Z. Liu, "Dft study on the mechanism of escherichia coli inorganic pyrophosphatase," *J. Phys. Chem. B*, vol. 113, pp. 6505–6510, 2009.
- [10] M. Fisher, "Quantum cognition: The possibility of processing with nuclear spins in the brain," *Annals of Physics*, vol. 362, pp. 593–602, 2015.
- [11] T. U. Consortium, "UniProt: a worldwide hub of protein knowledge," *Nucleic Acids Research*, vol. 47, pp. D506–D515, 11 2018.
- [12] V. Samygina, V. Moiseev, E. Rodina, N. Vorobyeva, A. Popov, S. Kurilova, T. Nazarova, S. Avaeva, and H. Bartunik, "Reversible inhibition of escherichia coli inorganic pyrophosphatase by fluoride: Trapped catalytic intermediates in cryo-crystallographic studies," *Journal of Molecular Biology*, vol. 336, no. 4, pp. 1305–1317.
- [13] J. Yang, R. Yan, A. Roy, D. Xu, J. Poisson, and Y. Zhang, "The i-tasser suite: Protein structure and function prediction," *Nature Methods*, vol. 12, pp. 7–8, 2015.
- [14] R. A. Kucukural and Y. A. Zhang, "I-tasser: a unified platform for automated protein structure and function prediction," *Nature Protocols*, vol. 5, pp. 725–738, 2015.
- [15] Y. Zhang, "I-tasser server for protein 3d structure prediction," *BMC Bioinformatics*, vol. 9, p. 40, 2008.
- [16] D. Case, I. Ben-Shalom, S. Brozell, D. Cerutti, T. Cheatham, V. Cruzeiro, T. Darden, R. Duke, D. Ghoreishi, M. Gilson, H. Gohlke, A. Goetz, D. Greene, R. Harris, N. Homeyer, S. Izadi, A. Kovalenko, T. Kurtzman, T. Lee, S. LeGrand, P. Li, C. Lin, J. Liu, T. Luchko, R. Luo, D. Mermelstein, K. Merz, Y. Miao, G. Monard, C. Nguyen, H. Nguyen, I. Omelyan, A. Onufriev, F. Pan, R. Qi, D. Roe, A. Roitberg, C. Sagui, S. Schott-Verdugo, J. Shen, C. Simmerling, J. Smith, R. Salomon-Ferrer, J. Swails, R. Walker, J. Wang, H. Wei, R. Wolf, X. Wu, L. Xiao, D. York, and P. Kollman, "Amber 2018," *University of California, San Francisco*, 2018.
- [17] L. T. Da, W. Dong, and X. Huang, "Dynamics of pyrophosphate ion release and its coupled trigger loop motion from closed to open state in rna polymerase ii," *J. Am. Chem. Soc.*, vol. 134, no. 4, pp. 2399–2406, 2012.
- [18] J. Maier, C. Martinez, K. Kasavajhala, L. Wickstrom, K. Hauser, and C. Simmerling, "Improving the accuracy of protein side chain and backbone parameters from ff99sb," *J. Chem. Theory Comput*, vol. 11, pp. 3696–3713, 2015.
- [19] P. Eastman, J. Swails, J. Chodera, R. McGibbon, Y. Zhao, and K. Beauchamp, "Openmm 7: Rapid development of high performance algorithms for molecular dynamics," *PLoS Comput Biol*, vol. 13, 2017.
- [20] C. J. Cramer, *Essentials of Computational Chemistry: Theories and Models*. West Sussex, England: Wiley, 2004.
- [21] W. Humphrey, A. Dalke, and K. Schulten, "Vmd - visual molecular dynamics," *J. Molec. Graphics*, vol. 14, pp. 33–38, 1996.
- [22] D. R. Roe and T. E. Cheatham, "Ptraaj and cptraaj: Software for processing and analysis of molecular dynamics trajectory data," *J. Chem. Theory Comput*, vol. 9, pp. 3084–9095, 2013.
- [23] R. T. e. a. McGibbon, "Mdtraj: A modern open library for the analysis of molecular dynamics trajectories," *Biophysical Journal*, vol. 109, no. 8, pp. 1528–1532.
- [24] S. van der Walt, S. C. Colbert, and G. Varoquaux, "The numpy array: A structure for efficient numerical computation," *Computing in Science & Engineering*, vol. 13, pp. 22–30, 2011.
- [25] matlab, "Matlab and statistics toolbox release 2012b," *The MathWorks, Inc. Natick, Massachusetts, United States*.
- [26] S. Krause, E. Willighagen, and C. Steinbeck, "Jchempaint – using the collaborative forces of the internet to develop a free editor for 2d chemical structures," *Molecules*, vol. 5, pp. 93–98, 200.

## 6. FIGURES

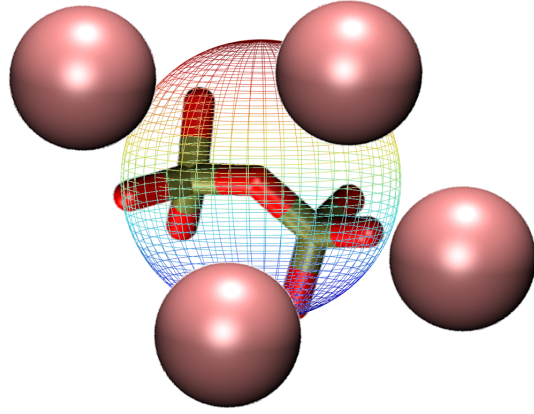


FIGURE 1. The singlet state's rotational freedom is approximated by the  $Y_0^0(\theta, \phi)$  spherical harmonic  $\left(Y_0^0(\theta, \phi) = \frac{1}{2}\sqrt{\frac{1}{\pi}}\right)$  [25].

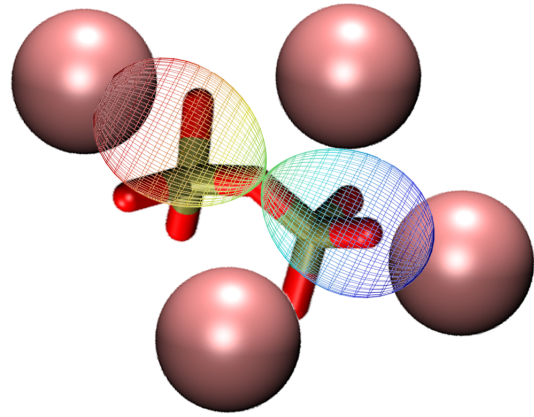


FIGURE 2. The triplet state's rotational freedom is approximated by the  $Y_0^1(\theta, \phi)$  spherical harmonic  $\left(Y_0^1(\theta, \phi) = \frac{1}{2}\sqrt{\frac{3}{2\pi}}\cos(\theta)\right)$  [25].

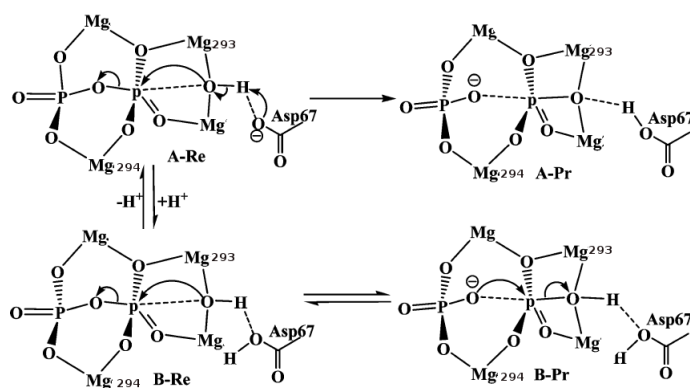


FIGURE 3. Brief overview of the proposed mechanism for the pyrophosphatase-catalyzed hydrolysis of  $PP_i$  (derived from [9] [26])

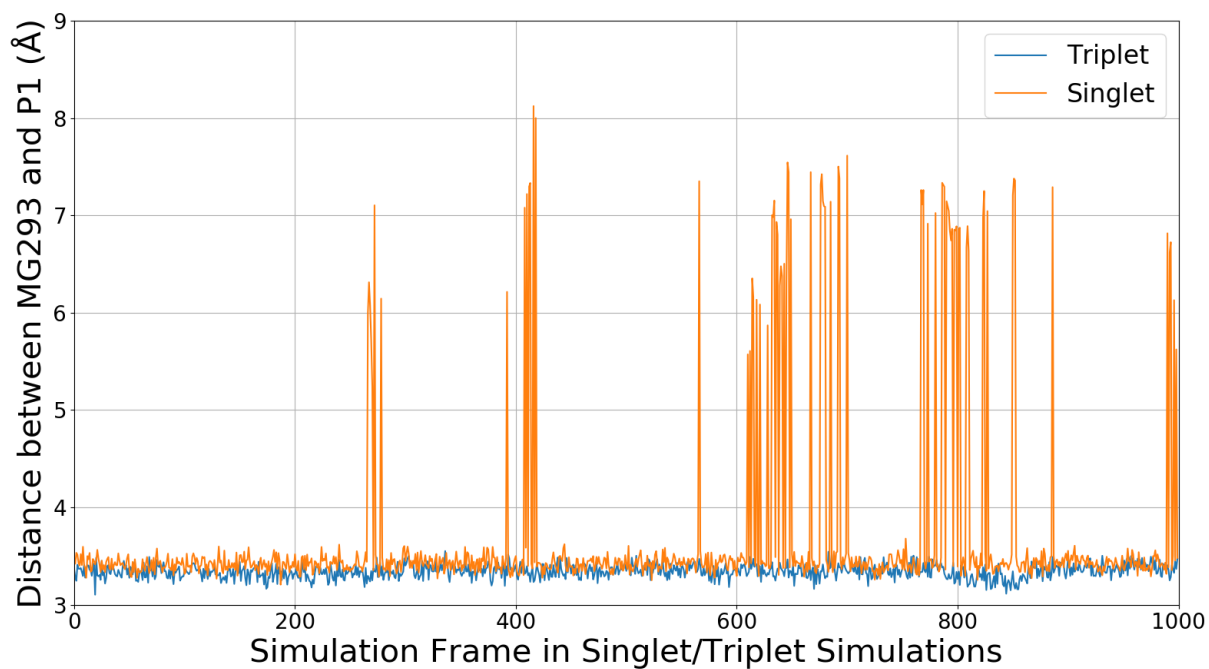


FIGURE 4. The distance between P1 and MG293 during the singlet (orange) and triplet (blue) NVT simulations. The peaks in the singlet simulation are due to the movement MG293 and not the rotation of  $PP_i$ .

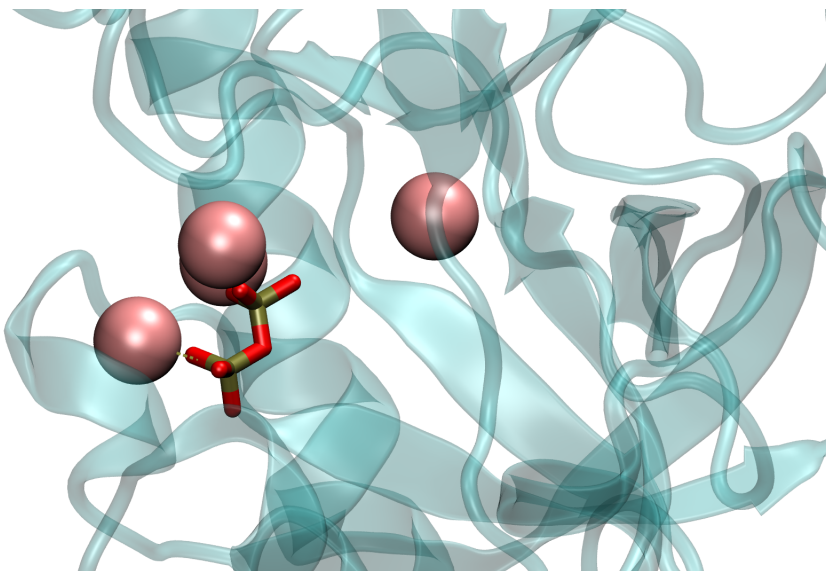


FIGURE 5. The distance between P1 and MG293 is 3.46 Å at frame 786 in the singlet NVT simulation.

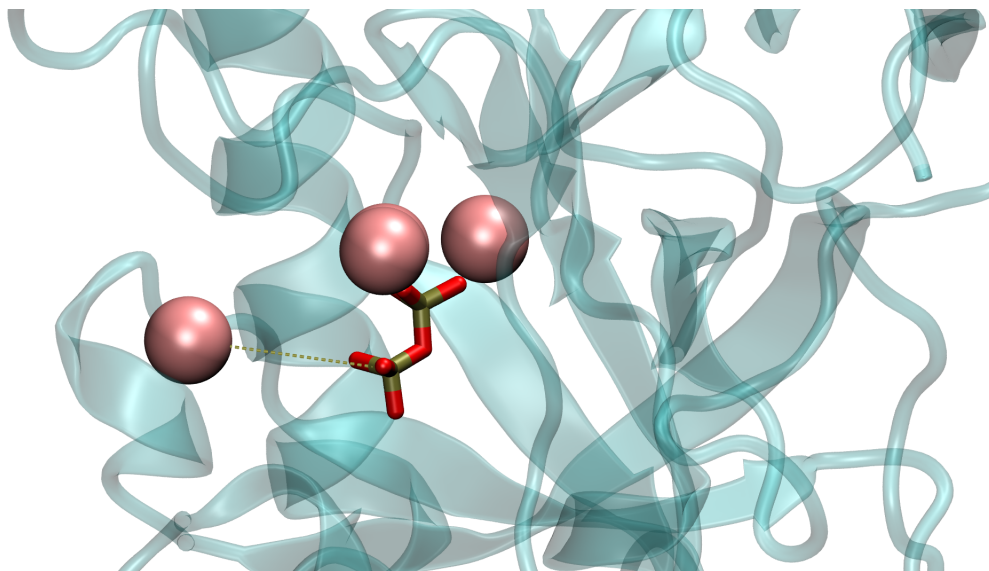


FIGURE 6. The distance between P1 and MG293 is 7.86 Å at frame 785 in the singlet NVT simulation.